Automatic Detection of Intracranial Aneurysm from Digital Subtraction Angiography with Cascade Networks

Junhua Liao
College of Computer Science, Sichuan University, Chengdu, 610065, China
junhua_liao@yeah.net

Haihan Duan
College of Computer Science, Sichuan University, Chengdu, 610065, China
duanhaihan@stu.scu.edu.cn

Huming Dai
College of Computer Science, Sichuan University, Chengdu, 610065, China
Huming_Dai@163.com

Yunzhi Huang
College of Electrical Engineering and Information Technology, Sichuan University, Chengdu, 610065, China
huang_yunzhi@scu.edu.cn

Lunxin Liu
West China Hospital, Sichuan University Department of Neurosurgery
liulunxin@hotmail.com

Liangyin Chen
College of Computer Science, The Institute for Industrial Internet Research, Sichuan University, Chengdu, 610065, China
chenliangyin@scu.edu.cn

Liangxue Zhou
West China Hospital, Sichuan University Department of Neurosurgery
Liangxue_zhou@126.com

ABSTRACT

Automatic detection of intracranial aneurysm based on Digital Subtraction Angiography (DSA) images is a challenging task for the following reasons: 1) effectively leverage the temporal information of the DSA sequence; 2) effectively extract features by avoiding unnecessary interference in the raw DSA images of large resolution; 3) effectively distinguish the vascular overlap from intracranial aneurysm in DSA images. To better identify intracranial aneurysm from DSA images, this paper proposed an automatic detection framework with cascade networks. This framework is consisted of a region localization stage (RLS) and an intracranial aneurysm detection stage (IADS). The RLS stage can significantly reduce the interference from unrelated regions and determine the coarse effective region. The IADS stage fully employed the spatial and temporal features to accurately detect aneurysm from DSA sequence. This method was verified in the posterior communicating artery (PCoA) region of internal carotid artery (ICA). In clinical trials, the accuracy of the baseline method was 62.5% with area under curve (AUC) of 0.650, and the time cost of the detection was approximately 62.546s. However, the accuracy of this method was 85.5% with AUC of 0.918, and the time cost of detection was about 3.664s. The experimental results showed that the proposed method significantly improved the accuracy and speed of intracranial aneurysm automatic detection.

AIPR 2019, August 16–18, 2019, Beijing, China

ACM ISBN 978-1-4503-7229-9/19/08…$15.00
DOI: https://doi.org/10.1145/3357254.3357258

CCS Concepts

•Computing methodologies → Artificial intelligence →Computer vision→Computer vision problems→Object detection

Keywords

Digital subtraction angiography; Intracranial aneurysm; Computer aided diagnosis; Object detection; Residual deep neural network; Bi-directional convolutional LSTM

1. INTRODUCTION

Intracranial aneurysm is a cerebrovascular disease that most scholars believe it is caused by congenital defects in the wall of the intracranial artery and increased intraluminal pressure. Without timely detection and treatment, the rupture of intracranial aneurysm often leads to severe neurological sequelae with high mortality[1]. Traditional diagnosis is usually performed by experienced physicians, but misdiagnosis or missing detection still occur from time to time. Therefore, using computer aided diagnosis (CAD) methods to help physicians identify aneurysm accurately and quickly can improve their work efficiency to a certain degree.

Recently, several systems based on magnetic resonance angiography (MRA) [2] and computed tomography angiography (CTA) [3] have been developed to automatically detect intracranial aneurysm. But the detection results of the MRA and the CTA can only be used as a reference indicator. Clinically, invasive digital subtraction angiography (DSA) is considered as the gold standard for aneurysm detection, because DSA has higher spatial resolution and sensitivity in detecting small aneurysm compared with MRA and CTA[4]. Thereinto, most existing CAD methods for aneurysm detection were based on 2D-DSA images due to the high cost of 3D angiography equipment. Abboud et al. [5] used morphology to predict the risk of rupture of intracranial

aneurysm. However, due to the lack of a method for automatically locating aneurysm, it can only be manually positioned by doctors. Rahmany et al. [6] combined fuzzy logic and expert prior knowledge to detect aneurysm. This method was limited by prior knowledge and could not cope with complex and diverse cases of aneurysm. Next, Rahmany et al. [7] combined the Zernike moments and the MSER detector to detect aneurysm on the vascular structure extracted by the Otsu method. Although the sensitivity of this work reached 100% on their test dataset, the false positive rate was as high as 78%. Subsequently, Rahmany et al. [8] combined with MSER, SURF and SIFT descriptors to detect aneurysm based on previous work [7], which relatively reduced the false positive rate. The detection methods proposed by Rahmany et al. have some limitations. First, these methods were based on the classical digital image processing (DIP) method which may not be the best way to extract features because it was susceptible to the interference from complex blood vessel distribution. Second, the angiographic images of DSA are time series, but the above-mentioned methods did not incorporate temporal information when detecting aneurysm. Third, the large resolution of raw 2D-DSA images not only influences the feature extraction, but also increases the computational cost.

In recent years, the residual deep neural network (ResNet) [9] and convolutional long short term memory (C-LSTM) [10] have performed well in feature extraction and image time information processing[11, 12]. Therefore, they have been gradually used in medical image processing, and achieved good results [13, 14, 15]. In order to better complete the detection of aneurysm, we combined ResNet and C-LSTM in our experiment. Thereinto, for better processing of temporal information, we used bi-directional C-LSTM (BDC-LSTM) which combined information of forward and backward streams as an output.

In this paper, we proposed a cascaded framework based on deep learning [16], which includes a region localization stage (RLS) and an intracranial aneurysm detection stage (IADS). The flowchart of our cascaded framework was shown in figure 1. The X_t^i meant the t^{th} frame in the raw DSA sequence of the i^{th} patient. The RLS was used to automatically locate a specific detection area, and the IADS performed aneurysm detection on the RLS positioning region. Three major contributions of this paper can be concluded as follows. First, we located a specific detection area through the RLS to reduce the background interference and computation time cost of the detection task compared with detection of the raw DSA images. Second, with the combination of the Feature Pyramid Networks (FPN) [17] with ResNet and BDC-LSTM as the backbone, the IADS combining spatial and temporal information greatly improved the accuracy and efficiency of aneurysm detection. Third, our method can achieve low false positive rate without false positive inhibition.

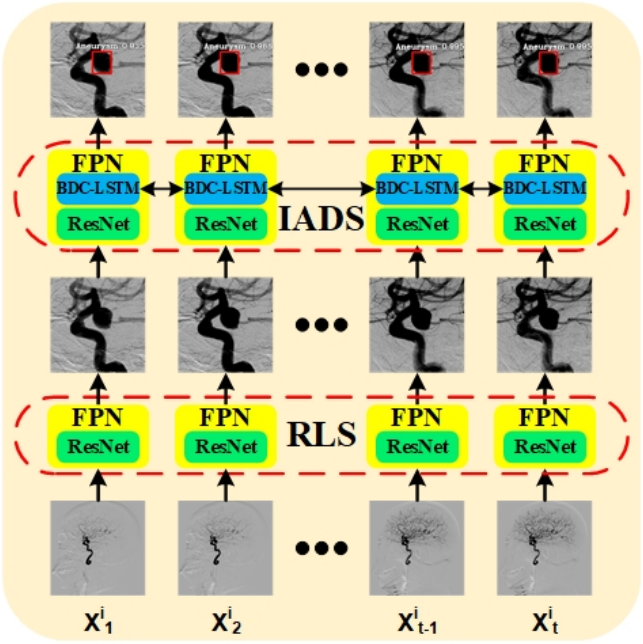

Figure 1. The flowchart of our cascaded framework.

2. METHOD

2.1 Region Localization Stage

The RLS was used to automatically locate specific detection region of raw 2D-DSA sequences, reducing interference and time loss for the IADS. The RLS could theoretically locate any region of ICA. But limited to the dataset, we only experimented on posterior communicating artery (PCoA) region. The network architecture of RLS was shown in figure 2. In RLS, a raw 2D-DSA sequence was used as input. The features of all frames in the DSA sequence were extracted by the FPN based on resnet50 [9] and sent to the anchor boxes [18] to predict PCoA region. The detector outputted 6n parameters. The number 6 represented the 6 parameters in the classification label, where the four parameters of the bounding-box (x, y, w, h, respectively representing the x-coordinate, y-coordinate, width and height) , classification and the confidence of the classification, and n meant the number of objects in the prediction result. Finally, the most confident prediction bounding-box were applied to other frames in the DSA sequence and output the PCoA region sequence. In order to connect with the IADS, we resized the image to 288×288.

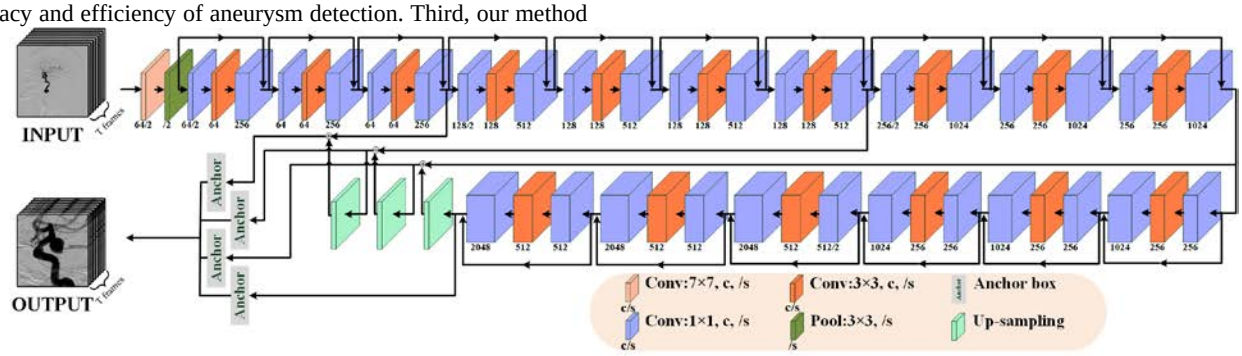

Figure 2. The network architecture of RLS.

Figure 2 shows the network architecture of RLS. In this figure, 'Conv：f×f, c, /s' meant a 2D convolutional layer with kernel size f×f, channel c and stride s. The stride defaulted to 1. And each convolutional layer was followed by a batch normalization (BN) [19] and an activation layer of ReLU [20]. 'Pool:f×f, /s' denoted max pooling layer whose size of filters was f and stride was s. 'Up－sampling' represented the nearest neighbor up-sampling with an up-sampling rate of 2. 'Anchor box' was used to predict the PCoA region.

2.2 Intracranial Aneurysm Detection Stage

The IADS was used to identify intracranial aneurysm. The network architecture of IADS was shown in figure 3. The DSA sequence $X = \{ X_t^i | t = 1,2,\ldots,T\}$ via RLS as input, where X_t^i represented the t^{th} frame in the DSA sequence of the i^{th} patient. The FPN extracted features based on resnet50 and BDC-LSTM. At first, we used resnet50 to extract features of each frame in the DSA sequence, and got the C3, C4 and C5 three-layer features. Next we were going to do time information processing. Although mono-directional C-LSTM (MDC-LSTM) was usually used to process the time information, this method made the time information obtained by each frame unequal. However, BDC-LSTM allowed each frame to obtain the time information of the entire sequence. In contrast, BDC-LSTM was more reasonable and reliable. So we sent the three-layer feature of C3, C4 and C5 to BDC-LSTM to get the information hidden in the time series. Finally, in order to better identify aneurysm of different sizes, we sent the three-layer feature containing spatial information and time information to FPN for further extraction. The extracted features were sent to the anchor boxes to detect aneurysm and overlap of blood vessels. The detector could predict 6n parameters which was identical with the RLS detector. The output retains objects with a confidence level higher than 0.6.

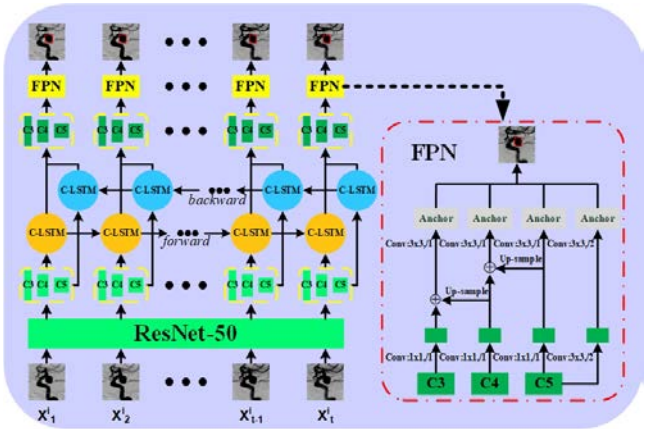

Figure 3. The network architecture of IADS.

Figure 3 shows the network architecture of IADS. In this figure, 'Conv：f×f, /s' meant a convolutional layer with kernel size f×f and stride s. The channel defaulted to 256. 'C3, C4, C5' represented three-layer features. 'Up－sample' indicated nearest neighbor up-sampling whose up-sampling rate was 2. 'Anchor' denoted anchor box which utilized the features to comp up the detection result.

2.3 Data

Our data set was obtained through neurosurgery of West China Hospital of Sichuan University, Chengdu, China. Experienced radiologists identified 8 consecutive frames form each patient's DSA sequences with sufficient visualization in PCoA region. A total of 540 DSA sequences from 270 patients, containing the frontal and lateral DSA sequences. The data set was divided into three parts. The first part was used to train RLS. We randomly selected 500 DSA sequences and manually labeled the PCoA region, 400 for training and 100 for testing. The second part included 500 DSA sequences to train resnet50 and BDC-LSTM respectively. These DSA sequences were obtained from the patients, who was diagnosed with aneurysm in PCoA region. When training resnet50, single frame images were used as input. DSA sequences were used as input when training BDC-LSTM. The third part including 40 DSA sequences, where 20 DSA sequences were diagnosed with aneurysm in PCoA region and other 20 DSA sequences were out of disease, which was used to evaluate our CAD system.

2.4 Training Process

All models were trained and tested with Keras [21] on NVIDIA GTX 1080Ti GPU(11GB GDDR5X). The training of the model was divided into three steps to train RLS, resnet50 and BDC-LSTM respectively. In order to achieve the local optimum better, we used the Adam Optimization method [22] during the training. The initial learning rate for each parts was 3×10^{-6}, 1×10^{-5} and 5×10^{-5}.

Focal Loss [17] was utilized as the loss function for object classification, which defined as

$$\mathrm{FL}(p,y) = \begin{cases} -\alpha(1-p)^{\gamma}\log p & y=1 \\ -\alpha\, p^{\gamma}\log(1-p) & otherwise \end{cases} \quad (1)$$

Where α denoted the balanced parameter, γ denoted the down-weighted rate, p denoted prediction confidence and $y \in \{\pm 1\}$ denoted the ground-truth class. We used $\alpha = 0.25$ and $\gamma = 2.0$ in the focal loss.

The loss function for bounding-box regression used Smooth L1 Loss [17], defined as follow,

$$\mathrm{SL}(t,v) = \sum_{i\in\{x,y,w,h\}} \mathrm{Smooth}_{\mathrm{L1}}(t_i - v_i) \quad (2)$$

in which,

$$\mathrm{Smooth}_{\mathrm{L1}}(x) = \begin{cases} 0.5(\sigma x)^2 & |x| < 1 \\ \dfrac{(|x|-0.5)}{\sigma^2} & \text{otherwise} \end{cases} \quad (3)$$

Where t denoted the bounding-box of predicted object, v denoted the bounding-box of ground-truth and σ denoted the weighted factor. We used $\sigma = 3.0$ in training process.

2.5 Performance Evaluation

To compare the MDC-LSTM model with the BDC-LSTM model, we used a 5-fold cross validation scheme with mean average precision (mAP) to assess the classification accuracy of intracranial aneurysm and overlap. The bounding-box regression task was evaluated by the Smooth L1 Loss.

In order to help doctors effectively identify intracranial aneurysm, we proposed a formula that determines whether the patient has intracranial aneurysm, defined as follows

$$Iaip^{n} = Iaip^{n}_{1F} \vee Iaip^{n}_{2F} \vee \ldots \vee Iaip^{n}_{(t-1)F} \vee Iaip^{n}_{tF} \vee Iaip^{n}_{1L} \vee Iaip^{n}_{2L} \vee \ldots \vee Iaip^{n}_{(t-1)L} \vee Iaip^{n}_{tL} \quad (4)$$

Where $Iaip^{n}$ denoted whether the n^{th} patient has intracranial aneurysm in PCoA region, $Iaip^{n}_{tF}$ and $Iaip^{n}_{tL}$ respectively represented whether the n^{th} patient detected intracranial aneurysm at the t^{th} frame in his DSA frontal or lat sequence. BDC-LSTM enables each frame in the DSA sequence to contain past and future information when it is detection. So in a patient's DSA frontal or lat sequence, the intracranial aneurysm is detected in any frame, we believe that the patient has intracranial aneurysm.

The confusion matrix and receiver operating characteristic (ROC) curve were used as evaluation methods. True positive (TP), true negative (TN), false positive (FP) and false negative (FN) are employed to calculate sensitivity, specificity and accuracy, which were defined as follows,

$$\text{Sensitive} = \text{True Positive Rate(TPR)} = \frac{TP}{TP + FN} \quad (5)$$

$$\text{Specificity} = \text{True Negative Rate(TNR)} = \frac{TN}{FP + TN} \quad (6)$$

$$\text{Accuracy} = \frac{TP + TN}{TP + FP + TN + FN} \quad (7)$$

Furthermore, the efficiency of the CAD system is also part of the assessment, which depends on the time cost of the calculation.

3. EXPERIMENTAL

3.1 Results

We used 100 DSA sequences to test the RLS with accuracy of 100%, which proved that our method can accurately locate the PCoA region. In figure 4, (a), (b) and (c) denote the raw DSA sequences, and (d), (e) and (f) represent the experimental results of RLS. In the IADS, we would evaluate the MDC-LSTM model and the BDC-LSTM model. The mAP results of 5-fold cross validation were shown in table 1. From the experimental results, the classification accuracy of MDC-LSTM is slightly better than BDC-LSTM. The Smooth L1 Loss of both MDC-LSTM and BDC-LSTM converges to around 0.3, which indicates that the boundary box regression accuracy of the results is higher.

Next, we selected 20 patients with aneurysm diagnosed in the PCoA area and 20 patients without aneurysm diagnosed in the PCoA area for clinical trials. Table 2(a) and table 2(b) respectively represent the confusion matrix for clinical trials using MDC-LSTM and BDC-LSTM. The confusion matrix for the replicated baseline method [8] is shown in table 2(c). The false negative of baseline method was only 1 case, but the false positive was up to 14 cases. Although the false negatives of MDC-LSTM were stable at 2.0 cases, the false positives were 7.2 cases and fluctuated greatly. In comparison, BDC-LSTM with a false negative rate of 2.4 cases and false positive rate of 3.4 cases performed better in overall performance.The ROC curve of MDC-LSTM and BDC-LSTM clinical trials are shown in figure 5(a) and figure 5(b), respectively. The BDC-LSTM has the highest average area under curve (AUC) of 0.918, compared to the baseline method with an AUC of 0.65 and the MDC-LSTM with an average AUC of 0.874.

Table 3 compares the model performance of the three methods. The sensitivity of the baseline method was as high as 0.950, but due to the specificity of 0.300, its accuracy was only 0.625. The MDC-LSTM with a sensitivity of 0.900 and a specificity of 0.640 showed a significant improvement in specificity, and it's accuracy also increased to 0.770. The BDC-LSTM maintains a relatively high sensitivity and further promotes specificity. It's accuracy rate can reach 85.5%. In terms of efficiency, the baseline method takes 62.546s to diagnose a patient. The MDC-LSTM and BDC-LSTM only need 5.014s and 3.664s respectively.

In summary, models using MDC-LSTM and BDC-LSTM are significantly better than the baseline approach. Compared with MDC-LSTM, BDC-LSTM performs better in all aspects except mAP. Therefore, we believe that the BDC-LSTM model is the best. The experimental results of IADS using BDC-LSTM are shown in figure 4 (g), (h) and (i). The red frame represents the aneurysm and the green frame denotes the overlap of the blood vessels.

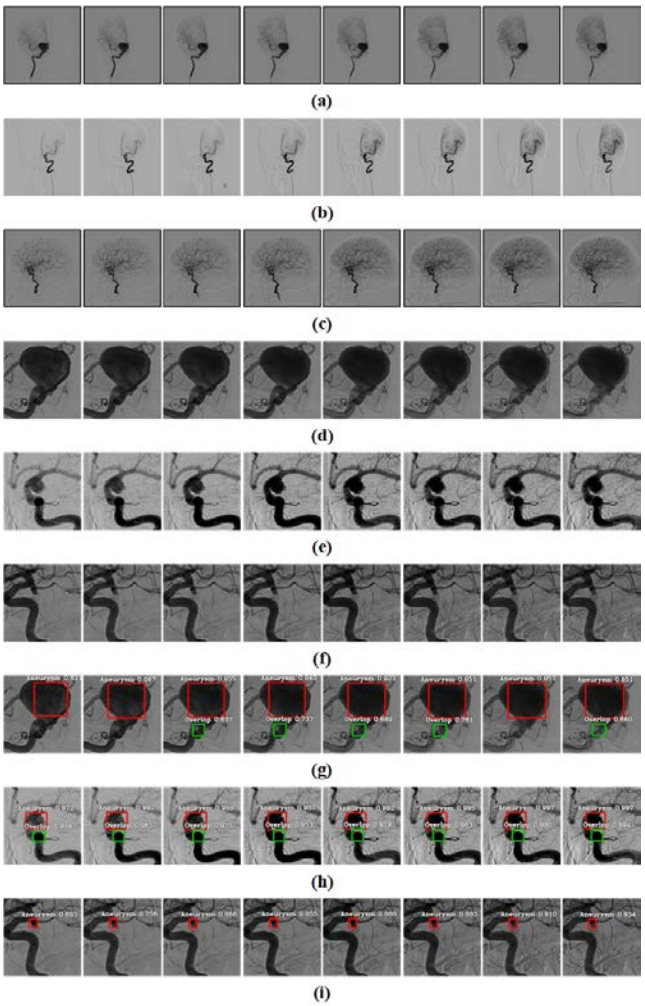

Figure 4. The results of RLS and IADS.

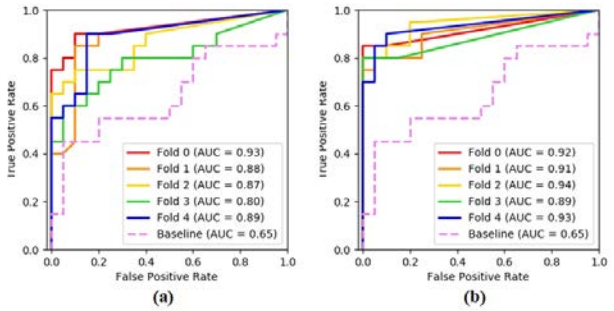

Figure 5. ROC curves of clinical trial with MDC-LSTM and BDC-LSTM.

Table 1. The mAP value of the 5-fold cross validation.

	Fold 0	Fold 1	Fold 2	Fold 3	Fold 4
MDC-LSTM	36.90%	60.11%	44.98%	62.15%	63.88%
BDC-LSTM	42.48%	55.53%	42.89%	57.68%	57.04%

Table 2. Confusion matrix for clinical trial using MDC-LSTM, BDC-LSTM and baseline method.

	Predict+	Predict-	Total
Diagnosis+	18.0 ± 0	2.0 ± 0	20
Diagnosis-	7.2 ± 3.66	12.8 ± 3.66	20
Total	25.2	14.8	40

(a)

	Predict+	Predict-	Total
Diagnosis+	17.6 ± 1.02	2.4 ± 1.02	20
Diagnosis-	3.4 ± 1.36	16.6 ± 1.36	20
Total	21	19	40

(b)

	Predict+	Predict-	Total
Diagnosis+	19	1	20
Diagnosis-	14	6	20
Total	33	7	40

(c)

Table 3. Comparison of the performance for each method.

Method	Sensitivity	Specificity	Accuracy	Time Cost
MDC-LSTM	0.900	0.640	0.770	5.014 ± 0.090 (s)
BDC-LSTM	**0.880**	**0.830**	**0.855**	**3.664 ± 0.028 (s)**
Baseline	0.950	0.300	0.625	62.546 ± 23.222 (s)

3.2 Analysis

Experimental results showed that the accuracy and speed of aneurysm detection can be greatly improved by locating the detection area on the large-resolution raw DSA images and combining the time and space information for aneurysm detection. Theoretically, the BDC-LSTM model is more reasonable than the MDC-LSTM model, because BDC-LSTM makes full use of time information, every image contains past and future information during detection. Therefore, the result of each frame has the same weights in diagnosis. But in MDC-LSTM, only the later frame can obtain more time information which is difficult to calculate the weights of each frame. The BDC-LSTM also performed better in clinical trial. In addition, our method achieved an accuracy of 0.855 without false-positive inhibition, whereas the baseline method with false-positive inhibition achieved an accuracy of 0.625. Of course, our experiment also has some limitations. First, our data set is small, with only 540 DSA sequences which did not contain the intracranial aneurysm in other ICA region. Second, the cascading network framework is relatively complex. However, it is difficult to detect such small aneurysms in the original DSA image with a resolution of 2000×2000. Third, due to the limited time, there are still many alternatives to try. In the future work, we are going to try different recurrent neural network architectures, such as the Time Convolutional Network [23].

4. CONCLUSION

This paper proposed a cascaded framework to detect intracranial aneurysm, including RLS and IADS. The RLS part demonstrated to be efficient in locating a specific detection region of the raw 2D-DSA sequence, which reducing interference from other tissues. In the IADS part, resnet50 was leveraged as backone to extract the representative features from each single frame of DSA sequence, and the BDC-LSTM module further extracted the temporal features from the DSA sequence. Based on the efficient and effective spatial and temporal features, the subsequent FPN block can detect intracranial aneurysm, and at the meanwhile to reduce the inference of the overlap of blood vessels. The results showed that the framework can help physicians identify intracranial aneurysm accurately and quickly.

5. ACKNOWLEDGMENTS

This paper is supported by National Natural Scientific Fund of China (81772693) and Science and Technology Department of Sichuan Province (19ZDYF0045 & 19CXTD0005). And thanks to the DSA data provided by neurosurgery of West China Hospital of Sichuan University, Chengdu, China.

6. REFERENCES

[1] Suarez, J. I., Tarr, R. W., and Selman, W. R. 2006. Aneurysmal subarachnoid hemorrhage. New England Journal of Medicine 354(4), 387 – 396.

[2] Hanaoka, S., Nomura, Y., Nemoto, M., Miki, S., Yoshikawa, T., Hayashi, N., Ohtomo, K., Masutani, Y., and Shimizu, A. 2015. Hotpig: A novel geometrical feature for vessel morphometry and its application to cerebral aneurysm detection. In: International Conference on Medical Image Computing and Computer-Assisted Intervention, pp. 103 – 110.

[3] Hentschke, C. M., Beuing, O., Paukisch, H., Scherlach, C., Skalej, M., and Tönnies, K. D. 2014. A system to detect cerebral aneurysms in multimodality angiographic data sets. Medical physics 41(9), 091904.

[4] Adams, W. M., Laitt, R. D., and Jackson, A. 2000. The role of mr angiography in the pretreatment assessment of intracranial aneurysms: a comparative study. American Journal of Neuroradiology 21(9), 1618 – 1628.

[5] Abboud, T., Rustom, J., Bester, M., Czorlich, P., Vittorazzi, E., Pinnschmidt, H. O., Westphal, M., and Regelsberger, J. 2017. Morphology of ruptured and unruptured intracranial aneurysms. World neurosurgery 99, 610 – 617.

[6] Rahmany, I., and Khlifa, N. 2017. A priori knowledge integration for the detection of cerebral aneurysm. Biomedical Engineering/Biomedizinische Technik 63(4), 445 – 452.

[7] Rahmany, I., Laajili, S., and Khlifa, N. 2018. Automated computerized method for the detection of unruptured cerebral aneurysms in dsa images. Current Medical Imaging Reviews 14(5), 771 – 777.

[8] Rahmany, I., Arfaoui, B., Khlifa, N., and Megdiche, H. 2018. Cerebral aneurysm computer-aided detection system by combing mser, surf and sift descriptors. In: 2018 5th International Conference on Control, Decision and Information Technologies (CoDIT), pp. 1122 – 1127.

[9] He, K., Zhang, X., Ren, S., and Sun, J. 2016. Deep residual learning for image recognition. In Proceedings of the IEEE Conference on Computer Vision and Pattern Recognition, pp. 770 – 778.

[10] Shi, X., Chen, Z., Wang, H., Yeung, D. Y., Wong, W. K., and Woo, W. C. 2015. Convolutional LSTM network: a machine learning approach for precipitation nowcasting.In Advances in neural information processing systems, pp. 802-810.

[11] Li, X., Zhao, H., and Zhang, L. 2018. Recurrent RetinaNet: A Video Object Detection Model Based on Focal Loss. In International Conference on Neural Information Processing, pp. 499-508.

[12] Chen, J., Yang, L., Zhang, Y., Alber, M., and Chen, D. Z. 2016. Combining fully convolutional and recurrent neural networks for 3d biomedical image segmentation. In Advances in neural information processing systems, pp. 3036-3044.

[13] Zisimopoulos, O., Flouty, E., Luengo, I., Giataganas, P., Nehme, J., Chow, A., and Stoyanov, D. 2018. DeepPhase: Surgical Phase Recognition in CATARACTS Videos. Lecture Notes in Computer Science, 265 – 272.

[14] Zheng, H., Gu, Y., Qin, Y., Huang, X., Yang, J., and Yang, G. Z. 2018. Small Lesion Classification in Dynamic Contrast Enhancement MRI for Breast Cancer Early Detection. Lecture Notes in Computer Science, 876 – 884.

[15] Bai, W., Suzuki, H., Qin, C., Tarroni, G., Oktay, O., Matthews, P. M., and Rueckert, D. 2018. Recurrent Neural Networks for Aortic Image Sequence Segmentation with Sparse Annotations. Lecture Notes in Computer Science, 586 – 594.

[16] Lecun, Y., Bengio, Y., and Hinton, G. 2015. Deep learning. Nature 521(7553): 436.

[17] Lin, T. Y., Goyal, P., Girshick, R., He, K., and Dollár, P. 2017. Focal loss for dense object detection. IEEE transactions on pattern analysis and machine intelligence.

[18] Ren, S., He, K., Girshick, R., and Sun, J. 2015. Faster r-cnn: Towards real-time object detection with region proposal networks. In: Advances in Neural Information Processing Systems, pp. 91 – 99.

[19] Ioffe, S. and Szegedy, C. 2015. Batch normalization: Accelerating deep network training by reducing internal covariate shift. arXiv preprint arXiv:1502.03167.

[20] Shang, W., Sohn, K., Almeida, D., and Lee, H. 2016. Understanding and improving convolutional neural networks via concatenated rectified linear units. In: International Conference on Machine Learning, pp. 2217 – 2225.

[21] Chollet, F., et al. 2018. Keras: The python deep learning library. Astrophysics Source Code Library.

[22] Kingma, D.P. and Ba, J. 2014. Adam: A method for stochastic optimization. arXiv preprint arXiv:1412.6980.

[23] Lea, C., Vidal, R., Reiter, A., and Hager, G.D. 2016. Temporal convolutional networks: a unified approach to action segmentation. In European Conference on Computer Vision, pp. 47 – 54.